ELSEVIER

Surface Science 331–333 (1995) 723–730

surface science

Structure and stability of fcc Fe films on Cu(100) for coverages below five monolayers

S. Müller, P. Bayer, A. Kinne, C. Reischl, R. Metzler, K. Heinz *

Lehrstuhl für Festkörperphysik, University of Erlangen-Nürnberg, Staudtstr. 7, D-91058 Erlangen, Germany

Received 29 July 1994; accepted for publication 11 November 1994

Abstract

The strong correlation between magnetism, growth and structure of ultrathin fcc Fe films on Cu(100) has caused much interest in these films recently. However, whilst the film structure has been extensively studied in the coverage regime $5 < \Theta < 10$ ml, the structural properties for lower coverages are only poorly known. We present LEED structure determinations of the 4×1 and 5×1 superstructures observed at coverages 2 and 4 ml, respectively. The results show that different from current assumptions the *entire* Fe films are heavily reconstructed. Atomic rows in the [110] direction buckle and shift in *all* iron layers leading to a complex film structure with atomic layers everything else but flat fcc (100) layers. So, in the coverage regime $\Theta < 5$ ml flat fcc (100) layers seem to be unstable and exhibit a highly distorted fcc structure. In addition, we find that all Fe interlayer distances are expanded which is nicely related to the ferromagnetic state of the films.

Keywords: Copper; Epitaxy; Iron; Low energy electron diffraction (LEED); Metallic films; Metallic surfaces; Metal–metal magnetic thin film structures; Surface relaxation and reconstruction; Surface structure

1. Introduction

The epitaxial growth of metals on metals offers the possibility to produce new materials with fascinating and unique properties. In particular the growth of Fe on Cu(100) allows to stabilize the fcc modification of allotropic Fe at room temperature (γ-Fe) which normally is stable only at higher temperatures ($1185 < T < 1667$ K). Earlier investigations of γ-Fe and Fe/Cu(100) [1–9] found strong correlations between the magnetic behaviour and the structural properties of Fe films. The majority of published structural analyses was concerned with the film structure between 5 and 10 monolayers (ml) [4,10–14], but there exists no precise structure determination for coverages $\Theta < 5$ ml. In this regime, two superstructures, 4×1 and 5×1, are reported [9,15–18], whereby the geometrical arrangement of atoms is largely unknown. However, the detailed knowledge of the atomic film structure is of importance for the qualitative and quantitative understanding of the film properties. So, for example films below 5 ml are ferromagnetic in the entire film whilst for thicker films ($5 \leqslant \Theta \leqslant 10$ ml) only the two top layers couple ferromagnetically [5] whereas the subsurface region shows antiferromagnetic coupling [19,20].

Therefore, we concentrate in the present paper on the coverage regime $\Theta < 5$ ml and present quantita-

* Corresponding author. Fax: +49 9131 858400; E-mail: kheinz@erympel.rrze.uni-erlangen.de.

SSDI 0039-6028(95)00217-0

tive structure determinations by low energy electron diffraction (LEED) for the 4×1 and 5×1 superstructures observed at 2 and 4 ml, respectively. It will be shown that the film structures are much more complex than assumed in an earlier LEED analysis [1]. For both superstructures the entire film is reconstructed whereby iron atoms possess enlarged atomic volumes of 12.1 Å^3 compared to the value of 11.4 Å^3 found for fcc Fe in the coverage regime $5 \leqslant \Theta \leqslant 10$ ml [4,10,11,13,14]. Therefore, the low coverage phase differs both magnetically and structurally from the bulk fcc-like structure of thicker Fe films [9]. Also, the structures found seem to mirror some instability of ultrathin γ-Fe films.

2. Experimental

The film preparation and LEED measurements were carried out in a standard ultrahigh vacuum system. Iron was evaporated from a reservoir of 4 N purity by electron bombardment and films were grown with the substrate held at 300 K. The coverage was calibrated both by a quartz microbalance and Auger electron spectroscopy. In the coverage regime up to about 5 ml complex LEED patterns develop as depicted in Fig. 1 for the 4×1 phase and the 5×1 phase at 2 and 4 ml, respectively. Films in the range between 2 and 3 ml show superstructure spots which cannot be assigned to $\frac{1}{4}$ or $\frac{1}{5}$ spot

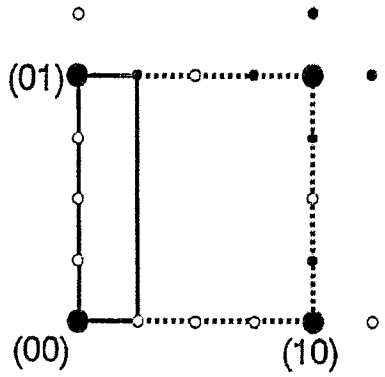

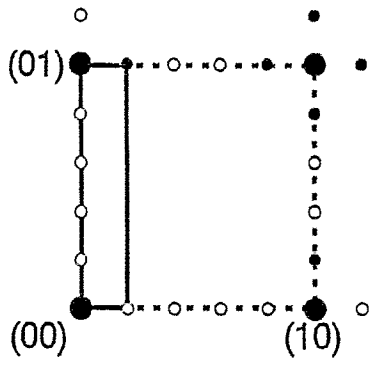

Fig. 1. Real and schematic LEED patterns at 2 and 4 ml coverage of Fe on Cu(100). Both LEED patterns were taken at 115 eV. Open circles in the schematic patterns indicate systematically weakened extra spots.

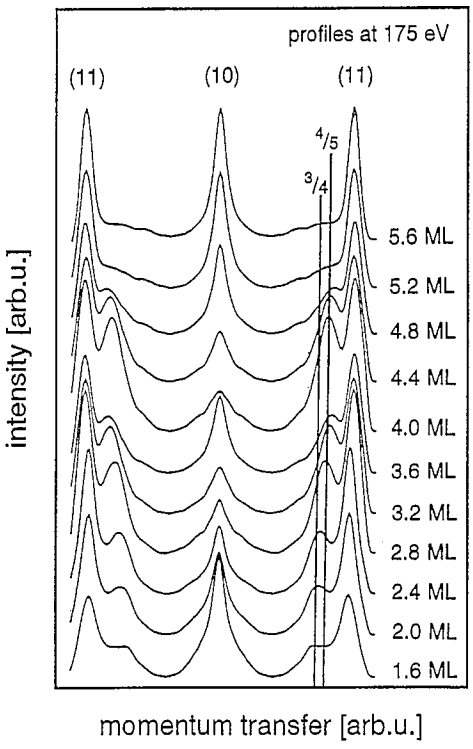

Fig. 2. Linear intensity profiles $I(k_p)$ taken at 90 K for various iron coverages. Vertical lines indicate $1\frac{3}{4}$ and $1\frac{4}{5}$ spot positions.

positions [9,17,21]. Generally, most of the extra spots are very weak and below the detection limit. Only those neighboured to substrate spots are visible but also weak, so that in case of the 4×1 phase they can be observed easily only at temperatures below 150 K. Spatial intensity profiles $I(k_p)$ taken at 90 K for various iron coverages as displayed in Fig. 2 demonstrate that the superstructure spots shift continuously from e.g. the $1\frac{3}{4}$ towards the $1\frac{4}{5}$ position during deposition of the 3rd Fe layer. So, whilst a pattern of 4×1 symmetry is only observed for $\Theta = 2$ ml, the 5×1 symmetry is typical for the regime 3–5 ml with $\frac{1}{5}$ superstructure spots being brightest at $\Theta = 4$ ml. With the coverage exceeding $\Theta = 5$ ml they disappear. Both the 4×1 and 5×1 patterns develop only for contamination-free films grown under UHV conditions with a residual gas pressure below 5×10^{-8} Pa. So, these phases must be regarded as intrinsic reconstructions of γ-Fe films [11].

For the quantitative analysis of the films intensity spectra $I(E)$ were taken for both the 4×1 phase at 2 ml and the 5×1 phase at 4 ml with the sample cooled to 90 K and carefully aligned to perpendicular incidence of the primary electron beam. A fast video-based technique as described in detail earlier [22,23] was used for data acquisition. The system collects LEED intensities via a video camera of high sensitivity operated under computer control. The video frame is digitized on-line and any linear profile as well as two-dimensional intensity maps can be recorded whereby high speed data averaging is supplied by adding up intensities of consecutive video half-frames. Also, integrated beam intensities can be measured by enframing a certain spot by a rectangular electronic window and integrating the inside intensities. The data are stored as function of electron energy whereby the moving spots are tracked under software control. This mode of measurement also includes on-line correction of background intensities which are determined at the window's edges. However, this procedure requires a spatially smooth variation of the background. It could be applied to measure the spectra of the integer order beams of both the 4×1 and the 5×1 phase, i.e. the 10, 11, 20, 21, 22 and their symmetrically equivalents. It was also applied to record the intensities of the fractional order beams of the 5×1 phase but failed to provide reliable data for the 4×1 superstructure spots. This is due to the very low intensity of the latter compared to the adjacent integer order beams as demonstrated by the intensity profile depicted in Fig. 3a. This profile was taken at an energy of 134 eV where both the 10 and $1\frac{1}{4}$ spots show maximum intensity (intensities averaged between 70 and 300 eV exhibit a ratio $I_{frac}/I_{int} \approx 0.02$). So, the "background intensities" of fractional order spots are dominated by the adjacent integer order spots. The background is comparable or even higher than the superstructure intensities and varies drastically with k_p. This makes the automated background correction mode described above fail, in particular when the electronic window, whose size is constant during the energy sweep, comes to overlap partly with the integer order beam at higher electron energies.

So an alternative but tedious method had to be chosen to get the intensity spectra of extra beams. Its major steps are demonstrated in Fig. 3. First, spatial intensity profiles (Fig. 3a) for the 4×1 phase were taken in steps of 2 eV in the range 70–300 eV. So, a total of 116 profiles of 220×3 pixels each were

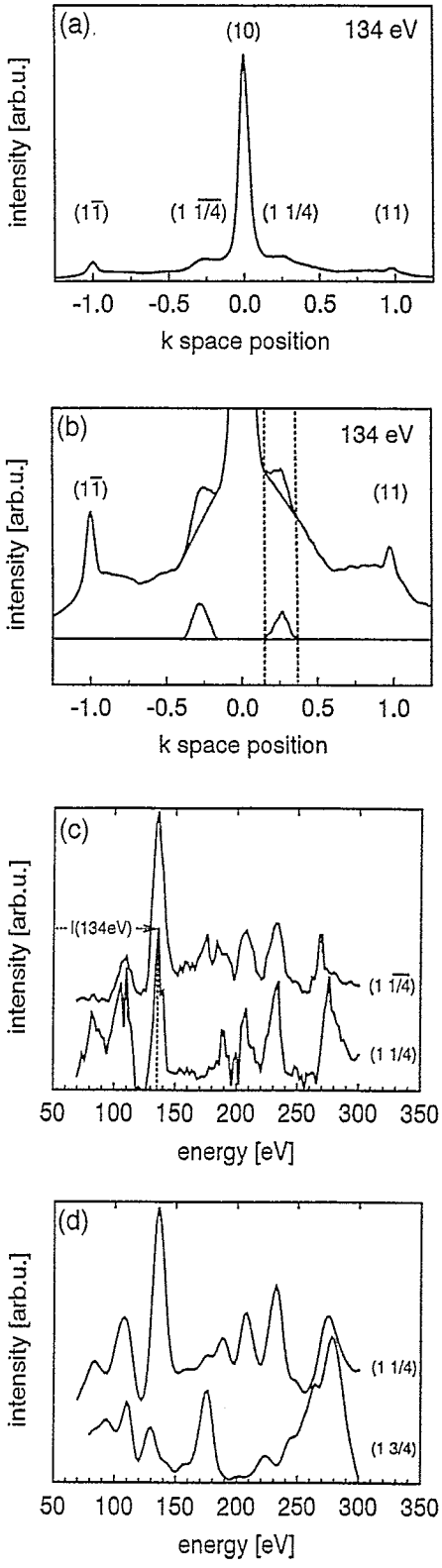

Fig. 3. Procedure of intensity data acquisition of superstructure beams of the 4×1 phase as described in the text: (a) spatial intensity profile; (b) background correction after linear interpolation; (c) resulting spectra of the $1\frac{1}{4}$ beam and its symmetrically equivalent and (d) $I(E)$ spectra of the $1\frac{1}{4}$ and $1\frac{3}{4}$ beams after averaging and smoothing.

recorded and stored on hard disc within a period of 30 min. Then the integrated intensity of the extra spots were evaluated off-line from the profiles by subtraction of "background intensities" determined by linear interpolation as displayed in Fig. 3b. In contrast to automated background subtraction, both the size and position of the interpolation interval can be adjusted at each energy by hand and under visual inspection. Each profile gives one single intensity/energy data point per superstructure spot as indicated in Fig. 3c. So, the evaluation of all 116 profiles finally produces the $I(E)$ spectra wanted. The procedure was carried out for the $1\frac{1}{4}$ and $1\frac{3}{4}$ beams and their symmetrically equivalents.

A visual inspection of the two equivalent spectra given in Fig. 3c reveals a comparably poor signal-to-noise ratio. However, both spectra show very similar shapes and the positions of major peak maxima coincide. In order to improve the data quality the spectra of symmetrically equivalent beams were averaged with subsequent three-point smoothing of the curves. Fig. 3d displays the resulting intensity spectra of the $1\frac{1}{4}$ and $1\frac{3}{4}$ beams as they were used as input to the structural analysis.

3. Intensity analysis

For a first structural search standard computer programs were applied [24,25] to calculate $I(E)$ spectra, while for the structural refinement the perturbation method Tensor LEED [26–28] was used. The calculations were restricted to a maximum energy of 300 eV in order to save computer time. The electron attenuation was simulated by an energy-dependent optical potential ($V_{0i} = 4.5$ eV at 90 eV). The real part of the inner potential was adjusted in the course of the theory–experiment fit as usual. For the quantitative fit procedure the Pendry R-factor R_p

was used [29], whereby the limits of errors were estimated by its variance $\mathrm{var}(R_p) = \sqrt{8V_{0i}/\Delta E}$ [29] with ΔE the total energy range used ($\Delta E = 1050$ eV/1200 eV for the 2 ml/4 ml film).

As mentioned above there is systematic weakening of most extra spots. This drastically restricts the number of possible structural models. Many models were tested, but only the two atomic arrangements shown in Fig. 4 reproduce the intensity levels mentioned. Model 2 could be excluded during the structural analysis, because no satisfying R-factor fit of the spectra could be obtained. So, only model 1 remained which was proposed earlier [30] and which corresponds to a distorted fcc(100) film with sine-like in-plane shifts of [110] atomic rows.

Variation of the first four interlayer distances for the sine model above does not lead to a good theory–experiment fit ($R_p > 0.6$ for both phases), when only the top layer is reconstructed. However, as described in more detail for the 5×1 phase in a separate paper [31] the fit drastically improves when the following structural modifications are introduced using Tensor LEED:

(i) If *all* layers are allowed to reconstruct sinusoidally the R-factor reduces to 0.40/0.45 for the $4 \times 1/5 \times 1$ superstructure, respectively.

(ii) Allowing for additional vertical buckling in all layers leads to $R_p = 0.18/0.14$.

A side view of the best fit models is given in Fig. 5. The atomic rows of all iron layers buckle and shift differently in each iron layer leading to a complex film structure. The best fit parameters are presented in Tables 1 and 2, whereby only the maximum buckling and shift amplitudes are given though the positions of all atoms of the film were determined. It is worth to note that as much as 40 parameters were adjusted in the structural refinement of the 5×1 phase. Independent variation of this large number of parameters can only be performed by an efficient perturbation method as Tensor LEED because full dynamical calculations with the need to treat each layer as composite layer would bring the necessary

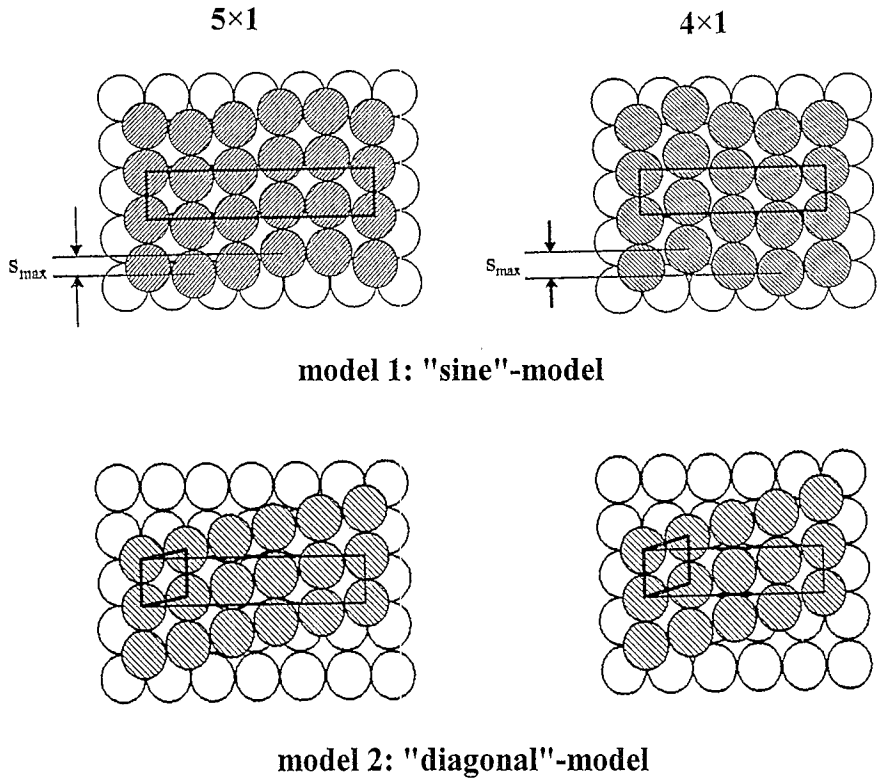

Fig. 4. Top view of possible structural models for the 4×1 and 5×1 phases.

computer time beyond any reasonable limits. However, the question arises, if the used data base is large enough for determination of 40 parameters. In the present case the total energy range used for the analysis of both phases was $\Delta E = 1200$ eV for the structure with the maximum number of parameters, i.e. the 5×1 phase. The width of a single maximum is of $\Delta E_s = 4V_{0i} \approx 24$ eV ($V_{0i} \approx 6$ eV as averaged over the energy range). If we assume each interference maximum to represent an independent piece of information the number of independent data points amounts to $n = \Delta E/\Delta E_s = 50$ which – as necessary – is larger than the number of structural parameters. Frequently, maxima come even nearer than estimated above, so the situation may be even more favourable.

Fig. 6 shows experimental and calculated best fit spectra for some selected beams of the 4×1 superstructure. Surprisingly, also for the fractional order spots of the 4×1 phase which were measured under difficult experimental conditions a good agreement between theory and experiment results (R_p(frac) = 0.31). Nevertheless, there remains a problem: Whilst for the 5×1 superstructure the complex film structure found fully accounts for the observed systematic weakening of most extra spots ($I_{strong}/I_{weak} = 800$), this is not the case for the 4×1 phase. Though the systematic weakening is reproduced by the starting structure, i.e. the model with sinusoidally reconstructed Fe layers, it is destroyed in the course of the R-factor fit procedure when vertical bucklings of the atomic layers are introduced. In particular, the best fit model of the 4×1 reconstruction produces $1\frac{2}{4}$ spot intensities comparable to those of the $1\frac{1}{4}$ and $1\frac{3}{4}$ spots, whilst no $1\frac{2}{4}$ superstructure spots are detected experimentally. However, we feel that this can be understood in terms of substantial disorder within the 2 ml film. As demonstrated in Fig. 1 the 4×1 LEED pattern exhibits more background and much weaker and more diffuse extra spots compared to the 5×1 phase. A possible explanation for the missing of the $1\frac{2}{4}$ spots is the coexistence of randomly distributed micro-domains with 4×1 structure. In-

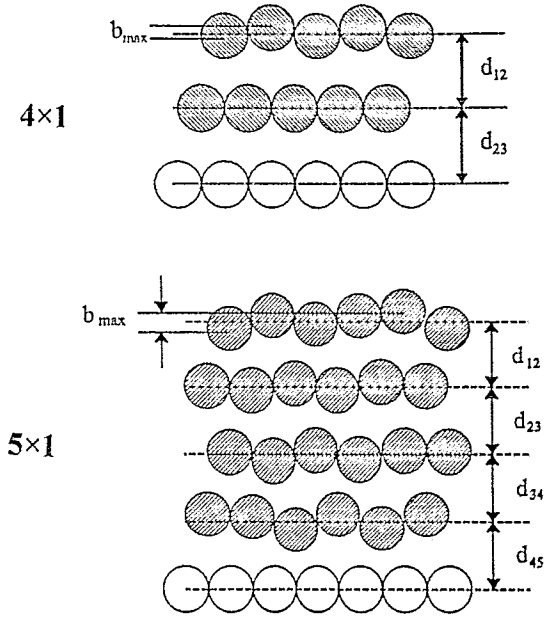

Fig. 5. Side views of the structural best fit models for the 4×1 and 5×1 phase.

Table 1
Best fit values of the structural parameters for the 5×1 phase

d_{12}	d_{23}	d_{34}	d_{45}
1.86 ± 0.02 (Å)	1.90 ± 0.02 (Å)	1.85 ± 0.03 (Å)	1.78 ± 0.06 (Å)
$\Delta d_{12}/d_0$	$\Delta d_{23}/d_0$	$\Delta d_{34}/d_0$	$\Delta d_{45}/d_0$
4.5 ± 1.1 (%)	6.5 ± 1.1 (%)	4.0 ± 1.7 (%)	0.0 ± 3.3 (%)
b_{max1}	b_{max2}	b_{max3}	b_{max4}
0.28 ± 0.02 (Å)	0.11 ± 0.02 (Å)	0.12 ± 0.03 (Å)	0.21 ± 0.05 (Å)
s_{max1}	s_{max2}	s_{max3}	s_{max4}
0.40 ± 0.10 (Å)	0.30 ± 0.15 (Å)	0.30 ± 0.20 (Å)	0.40 ± 0.30 (Å)

The quantity d_0 denotes the bulk interlayer distance of fcc Fe as extrapolated from the equilibrium high temperature phase.

Table 2
Best fit values of the structural parameters for the 4×1 phase.

d_{12}	d_{23}
1.87 ± 0.02 (Å)	1.84 ± 0.02 (Å)
$\Delta d_{12}/d_0$	$\Delta d_{23}/d_0$
5.0 ± 1.1 (%)	3.5 ± 1.1 (%)
b_{max1}	b_{max2}
0.18 ± 0.02 (Å)	0.04 ± 0.02 (Å)
s_{max1}	s_{max2}
0.50 ± 0.10 (Å)	0.30 ± 0.20 (Å)

deed, the superposition of the scattering amplitudes for two (4×1) domains shifted by one substrate lattice constant with respect to each other leads to an extinction of the $1\frac{2}{4}$ spots whereas experimentally visible superstructure spots are preserved. So, assuming the diameter of the domains being smaller than the coherence length of the electron beam no $1\frac{2}{4}$ spots appear in the LEED pattern in agreement with experiment. Further support for this interpretation comes by the following observation: Annealing the film at 400 K, which was avoided before in order to exclude copper segregation [32], seems to increase the crystallographic order of the 4×1 phase considerably. Not only the initial superstructure spots get sharper and more intense, but also $1\frac{2}{4}$ spots appear. Consequently, the latter must be produced by the 4×1 reconstruction and appear during the structural ordering of the film when the domains grow in size. So, the above structural analysis of the 4×1 phase seems to be reliable. Particularly, the major findings,

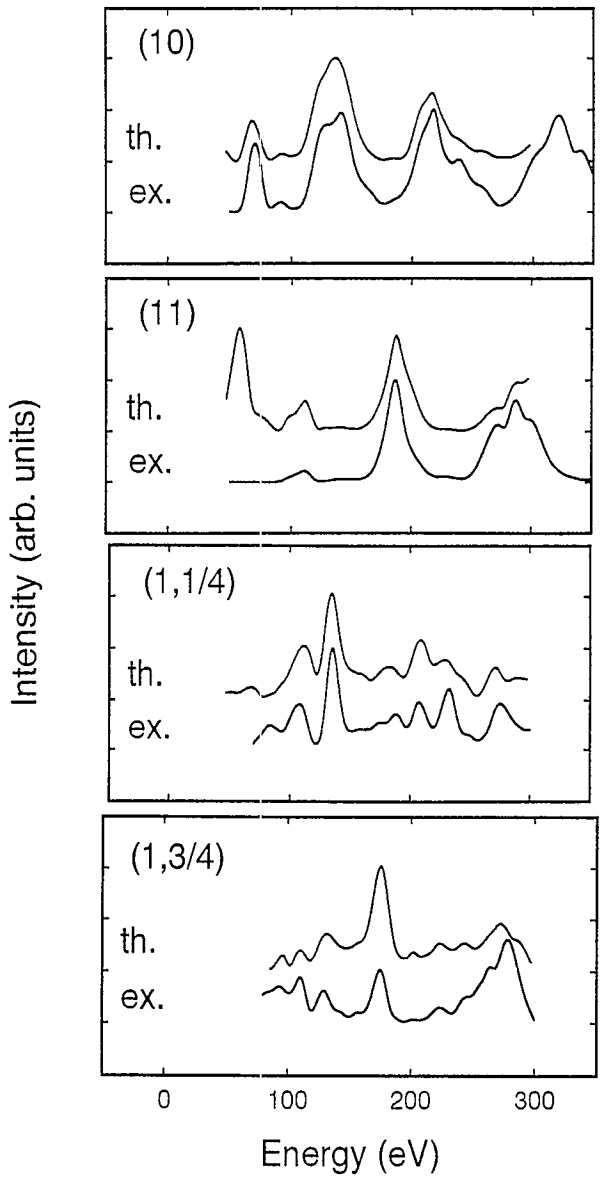

Fig. 6. Selected experimental and calculated best fit spectra for the 4×1 phase.

namely a complex reconstruction of the film and a drastic expansion of the Fe interlayer distance similar to the 5×1 phase are on safe grounds.

4. Discussion

The above structure determinations show that the structural properties of Fe films for coverages lower than 5 ml are very different from those found for fcc iron films between 5 and 10 ml. The Fe layers are everything else but flat fcc (100) layers. All layers are reconstructed by horizontal and vertical atomic shifts leading to a substantial restructuring of the whole iron film, i.e. to a highly distorted fcc structure. Consistent with the reconstruction all interlayer distances are expanded corresponding to an average atomic volume of about 12.1 Å^3. This is substantially larger than the value of 11.4 Å^3 found for thicker iron films in the coverage regime 5–10 ml [4,10,11,13,14]. In view of first principle calculations which predict an increased atomic volume for ferromagnetic coupling [3] these findings are in nice agreement with the magnetic properties of the films. While for $5 \leqslant \Theta \leqslant 10$ ml antiferromagnetic coupling is found in the interior of the film, in the low coverage regime ($\Theta < 5$ ml) the entire iron film is ferromagnetic [5,9,19,20]. Also, the 4×1 and 5×1 reconstructions show that the pure fcc Fe modification is not stable in the coverage regime $\Theta < 5$ ml. The structures found are fcc only on average. Our results request that earlier theoretical investigations of Fe/Cu(100) assuming flat fcc(100) Fe layers should be repeated allowing for appropriate film reconstruction.

Acknowledgements

We gratefully acknowledge support by Deutsche Forschungsgemeinschaft (DFG).

References

[1] A. Clarke, P.J. Rous, M. Arnott, G. Jennings and R.F. Willis, Surf. Sci. 192 (1987) L843.
[2] V.L. Moruzzi, P.M. Marcus, K. Schwarz and P. Mohn, Phys. Rev. B 34 (1986) 1784.
[3] V.L. Moruzzi, P.M. Marcus and J. Kübler, Phys. Rev. B 39 (1989) 6957.
[4] P. Bayer, S. Müller, P. Schmailzl and K. Heinz, Phys. Rev. B 48 (1993) 17611.
[5] J. Thomassen, F. May, B. Feldmann, M. Wuttig and H. Ibach, Phys. Rev. Lett. 69 (1992) 3831.
[6] S.H. Lu, J. Quinn, D. Tian, F. Jona and P.M. Marcus, Surf. Sci. 209 (1989) 364.
[7] T. Kraft, P.M. Marcus and M. Scheffler, Phys. Rev. Lett., submitted.
[8] D.P. Pappas, C.R. Brundle and H. Hopster, Phys. Rev. B 45 (1992) 8169.
[9] S. Müller, P. Bayer, C. Reischl, K. Heinz, B. Feldmann, H. Zillgen and M. Wuttig, Phys. Rev. Lett. 74 (1995) 765.
[10] S. Müller, P. Bayer, A. Kinne, P. Schmaizl and K. Heinz, Surf. Sci. 322 (1995) 21.
[11] M. Wuttig and J. Thomassen, Surf. Sci. 282 (1993) 273.
[12] H. Landskron, G. Schmidt, K. Heinz, K. Müller, C. Stuhlmann, U. Beckers, M. Wuttig and H. Ibach, Surf. Sci. 256 (1991) 115.
[13] H. Magnan, D. Chandesris, B. Villette, O. Heckmann and J. Lecante, Phys. Rev. Lett. 67 (1991) 859.
[14] H. Magnan, D. Chandesris, B. Villette, O. Heckmann and J. Lecante, Surf. Sci. 251/252 (1991) 597.
[15] J. Thomassen, B. Feldmann and M. Wuttig, Surf. Sci. 264 (1992) 406.
[16] C. Egawa, E.M. McCash and R.F. Willis, Surf. Sci. 215 (1989) L271.
[17] P. Xhonneux and E. Courtens, Phys. Rev. B 46 (1992) 556.
[18] M.T. Kief and W.F. Egelhoff, Phys. Rev. B 47 (1993) 10785.
[19] W.A. Macedo and W. Keune, Phys. Rev. Lett. 61 (1988) 475.
[20] D. Li, M. Freitag, J. Pearson, Z.Q. Qiu and S.D. Bader, Phys. Rev. Lett. 72 (1994) 3112.
[21] D.P. Pappas, K.-P. Kämper, B.B. Miller, H. Hopster, D.E. Fowler, A.C. Luntz, C.R. Brundle and Z.-X. Shen, J. Appl. Phys. 69 (1991) 5209.
[22] K. Müller and K. Heinz, in: The Structure of Surfaces, Vol. 2 of Springer Series in Surface Science, Eds. M.A. Van Hove and S.Y. Tong (Springer, Berlin, 1986) p. 105.
[23] K. Heinz, Progr. Surf. Sci. 27 (1988) 239.
[24] J.B. Pendry, Low Energy Electron Diffraction (Academic Press, London, 1974).
[25] M.A. Van Hove and S.Y. Tong, Surface Crystallography by LEED (Springer, Berlin, 1979).
[26] P.J. Rous, J.B. Pendry, D.K. Saldin, K. Heinz, K. Müller and N. Bickel, Phys. Rev. Lett. 57 (1986) 2951.
[27] P.J. Rous and J.B. Pendry, Surf. Sci. (1989) 219, 355 and 373.
[28] P.J. Rous, Progr. Surf. Sci. 39 (1992) 3.
[29] J.B. Pendry, J. Phys. C 13 (1980) 937.
[30] W. Daum, C. Stuhlmann and H. Ibach, Phys. Rev. Lett. 60 (1988) 2741.
[31] K. Heinz, S. Müller and P. Bayer, Surf. Sci., accepted for publication.
[32] D.A. Steigerwald, I. Jacob and W.F. Egelhoff, Jr., Surf. Sci. 202 (1988) 472.